

Structures of *Helicobacter pylori* uridylate kinase: insight into release of the product UDP

Chen-Hsi Chu,^{a,b} Mu-Hsuan Liu,^a
Pin-Chen Chen,^a Ming-Hsing
Lin,^a Yi-Chuan Li,^a Chwan-Deng
Hsiao^b and Yuh-Ju Sun^{a*}

^aInstitute of Bioinformatics and Structural
Biology, National Tsing Hua University,
Hsinchu 300, Taiwan, and ^bInstitute of
Molecular Biology, Academia Sinica,
Taipei 115, Taiwan

Correspondence e-mail: yjsun@life.nthu.edu.tw

Uridylate kinase (UMPkin; EC 2.7.4.22) transfers the γ -phosphate of ATP to UMP, forming UDP. It is allosterically regulated by GTP. Structures of *Helicobacter pylori* UMPkin (HpUMPkin) complexed with GTP (HpUMPkin-GTP) and with UDP (HpUMPkin-UDP) were determined at 1.8 and 2.5 Å resolution, respectively. As expected, HpUMPkin-GTP forms a hexamer with six GTP molecules at its centre. Interactions between HpUMPkin and GTP are made by the β 3 strand of the sheet, loop β 3 α 4 and the α 4 helix. In HpUMPkin-UDP, the hexameric symmetry typical of UMPkins is absent. Only four of the HpUMPkin molecules bind UDP; the other two HpUMPkin molecules are in the UDP-free state. The asymmetric hexamer of HpUMPkin-UDP, which has an exposed dimer interface, may assist in UDP release. Furthermore, the flexibility of the α 2 helix, which interacts with UDP, is found to increase when UDP is absent in HpUMPkin-UDP. In HpUMPkin-GTP, the α 2 helix is too flexible to be observed. This suggests that GTP binding may affect the conformation of the α 2 helix, thereby promoting UDP release.

Received 20 December 2011
Accepted 15 March 2012

PDB References: HpUMPkin-GTP, 4a7w; HpUMPkin-UDP, 4a7x.

1. Introduction

Nucleotides are necessary for DNA and RNA synthesis: they are energy sources and are involved in signal transduction and cellular metabolism, and their levels are also controlled by the actions of many different enzymes; for example, carbamoyl phosphate synthetase, nucleoside monophosphate (NMP) kinases, nucleoside diphosphate kinases and CTP synthase (Stevens, 1963; Shambaugh, 1979; Yan & Tsai, 1999). Genes encoding NMP kinases have been cloned and sequenced, and the biochemical properties and structural features of NMP kinases from several organisms have been studied (Jong *et al.*, 1993; Serina *et al.*, 1995, 1996; Yan & Tsai, 1999). Two main classes of NMP kinases, class I and class II, have been defined. Class I NMP kinases (~200 residues) are monomeric and contain a Rossmann fold (Rossmann *et al.*, 1974) and a strictly conserved P-loop sequence (GX₄GKT; Schulz, 1987; Saraste *et al.*, 1990; Labesse *et al.*, 2011). Class II NMP kinases (~240 residues) are hexamers and contain the KX₃₈₋₄₂GGGN motif (Labesse *et al.*, 2011). Eukaryotic bifunctional UMP/CMP kinases belong to class I and efficiently phosphorylate both UMP and CMP (Müller-Dieckmann & Schulz, 1994; Liou *et al.*, 2002; Schulz, 1987; Zhou & Thornburg, 1998). Bacterial UMP kinases are class II enzymes; although they also contain a Rossmann fold, they do not contain many of the other distinguishing class I structural features and they only phosphorylate UMP (Yan & Tsai, 1999; Labesse *et al.*, 2011).

Table 1

X-ray diffraction data-collection and refinement statistics for *Hp*UMPK–GTP and *Hp*UMPK–UDP.

Values in parentheses are for the highest resolution shell.

Crystal	<i>Hp</i> UMPK–GTP	<i>Hp</i> UMPK–UDP
Data-collection statistics		
Source	NSRRC 13B1	
Wavelength (Å)	1.000	0.979
Space group	<i>R</i> 32	<i>C</i> 2
Resolution (Å)	1.8 (1.86–1.80)	2.5 (2.54–2.45)
Unit-cell parameters		
<i>a</i> (Å)	137.4	147.2
<i>b</i> (Å)	137.4	127.6
<i>c</i> (Å)	152.9	93.2
β (°)		91.5
No. of reflections	568468	233702
No. of unique reflections	51426 (5109)	62731 (6175)
Multiplicity	11.1	3.7
Completeness (%)	99.5 (100.0)	99.6 (98.8)
$\langle I/\sigma(I) \rangle$	37.3 (4.2)	21.3 (2.3)
$R_{\text{merge}}^{\dagger}$ (%)	6.7 (50.0)	5.7 (52.8)
Refinement statistics		
Resolution (Å)	25.0–1.8	30.0–2.5
R factor \ddagger / R_{free}^{\S} (%)	19.0/22.7	21.3/27.6
No. of reflections in working set	51379	56433
No. of reflections in test set	2612	2994
No. of protomers in asymmetric unit	2	6
No. of residues	452	1381
No. of protein atoms	3428	10464
No. of water molecules	316	393
R.m.s.d. bond lengths (Å)	0.006	0.008
R.m.s.d. bond angles (°)	1.038	1.208
Average <i>B</i> factors (Å ²)		
All protein atoms	25.2	51.4
UDP	n/a	48.6
GTP	17.5	n/a
Glycerol	26.7	n/a
Water molecules	28.7	55.8
Overall	25.4	51.5
<i>MolProbity</i> validation		
Ramachandran plot (%)		
Favoured	97.5	97.2
Allowed	2.5	2.8

$\dagger R_{\text{merge}} = \sum_{hkl} \sum_i |I_i(hkl) - \langle I(hkl) \rangle| / \sum_{hkl} \sum_i I_i(hkl)$, where $\langle I(hkl) \rangle$ is the mean of the individual measurements $I_i(hkl)$ of the intensity of reflection hkl . $\ddagger R = \sum_{hkl} ||F_{\text{obs}}| - |F_{\text{calc}}|| / \sum_{hkl} |F_{\text{obs}}|$, where F_{obs} and F_{calc} are the observed and calculated structure-factor amplitudes, respectively. $\S R_{\text{free}}$ was calculated using 5% of the total number of reflections randomly omitted from the refinement.

UMP is synthesized by *de novo* and salvage pathways (Shambaugh, 1979; Neuhaard & Kelln, 1996). The subsequent transfer of an ATP γ -phosphate to UMP by UMP kinase (UMPK) yields UDP, which is the biosynthetic precursor for all other pyrimidine nucleotides (Neuhaard & Kelln, 1996). As the rate-limiting enzyme in nucleotide biosynthesis (Humeniuk *et al.*, 2009), UMPKs are feedback-inhibited by UTP (Serina *et al.*, 1996) and positively allosterically regulated by GTP (Serina *et al.*, 1996; Fassy *et al.*, 2004; Gagy *et al.*, 2003).

Other regulatory mechanisms for UMPKs differ in different species. For *Escherichia coli* UMPK (*Ec*UMPK), Mg^{2+} reverses inhibition by UTP but does not affect activation by GTP (Briozzo *et al.*, 2005). When Mn^{2+} is bound to *Helicobacter pylori* UMPK (*Hp*UMPK), the enzyme is activated by a lower concentration of GTP than other bacterial UMPKs (Lee *et al.*, 2010). UMPKs from *E. coli*, *Haemophilus influenzae*

and *Streptococcus pneumoniae* are essential for cell survival (Yamanaka *et al.*, 1992; Akerley *et al.*, 2002; Fassy *et al.*, 2004). As an example, *S. pneumoniae* cannot grow normally when the *pyrH* gene (which encodes the UMPK protein) is knocked out, but the survival of *S. pneumoniae* can be complemented by the *Bacillus subtilis cmk* gene encoding the CMPK protein, which also has UMPK activity. Additionally, an *E. coli* strain carrying a disrupted *smbA* gene, which has been described as *pyrH*, on the chromosome can be transduced by a phage into the *smbA*⁺ strain but not into the non-*smbA*⁺ strain. Hence, the UMPK of *H. pylori* might also be essential for survival and be a target for antibacterial drug development, as *H. pylori* has been linked to chronic gastritis, gastric and duodenal ulcers and stomach cancer. Consequently, the structure and the relationships between the catalytic and allosteric mechanisms of *Hp*UMPK need to be delineated. In the study reported here, we solved the crystal structures of *Hp*UMPK complexed with GTP (*Hp*UMPK–GTP) and with UDP (*Hp*UMPK–UDP) at 1.8 and 2.5 Å resolution, respectively. By comparing the two structures, we were able to propose a mechanism for the allosteric regulation of *Hp*UMPK by GTP. The *Hp*UMPK structures provide a novel platform for the development of new drug candidates for *H. pylori* that target nucleotide-biosynthetic pathways.

2. Materials and methods

2.1. Protein expression, purification and crystallization

The cloning and purification of *Hp*UMPK have been reported previously (Lee *et al.*, 2010). The PCR product of the UMPK gene (723 bp) from *H. pylori* 26695 genomic DNA was ligated into the *Bam*HI and *Sal*I sites of pQE30 (Qiagen), which added 12 residues at the N-terminus including a hexahistidine tag (MRGSHHHHHHGS). Cells transformed with the pQE30-*Hp*UMPK expression vector were cultured overnight at 310 K in Luria–Bertani medium with 50 $\mu\text{g ml}^{-1}$ ampicillin and 25 $\mu\text{g ml}^{-1}$ kanamycin. 10 ml samples of the overnight culture were then individually added to 1 l aliquots of fresh Luria–Bertani medium and these cultures were incubated at 310 K and 160 rev min^{−1} until their OD₆₀₀ values reached 0.6–1.0. The expression of *Hp*UMPK was induced by adding isopropyl β -D-1-thiogalactopyranoside (final concentration 1 mM) at 310 K. The cultures were then incubated for an additional 4 h. A cell pellet was obtained by centrifugation (6000g) and was dissolved in 40 ml 20 mM Tris pH 9.0, 300 mM NaCl, 10% glycerol, 1 mM UDP. The cell suspension was homogenized with a high-pressure homogenizer (EmulsiFlex-C5, Avestin Incorporation). The lysate was clarified by centrifugation (24 000g) at 277 K for 15 min. The supernatant was loaded onto an Ni–NTA column (GE Healthcare). *Hp*UMPK was eluted with 20 mM Tris pH 9.0, 300 mM NaCl, 300 mM imidazole, 10% glycerol, 1 mM UDP. The yield of *Hp*UMPK was ~20 mg per litre of culture. The N-terminal hexahistidine tag remained on *Hp*UMPK during the crystallization experiment.

*Hp*UMP_K–GTP and *Hp*UMP_K–UDP crystals were grown by the hanging-drop vapour-diffusion method. For the crystallization of *Hp*UMP_K–GTP, 1 µl 5 mg ml^{−1} *Hp*UMP_K (in 20 mM Tris pH 9.0, 300 mM NaCl, 300 mM imidazole, 10% glycerol, 1 mM UDP, 1 mM ATP, 5 mM GTP) and 1 µl reservoir solution (150 mM sodium acetate pH 4.8, 270 mM ammonium sulfate, 18% PEG MME 550) were mixed and equilibrated against reservoir solution (500 µl) at 284 K. *Hp*UMP_K–GTP crystals formed within 6 d and grew to dimensions of 0.3 × 0.3 × 0.3 mm.

For the crystallization of *Hp*UMP_K–UDP, 1 µl 5 mg ml^{−1} *Hp*UMP_K (in 20 mM Tris pH 9.0, 300 mM NaCl, 300 mM imidazole, 10% glycerol, 1 mM UDP) and 1 µl reservoir solution (0.15 M sodium acetate pH 4.8, 0.35 M ammonium

sulfate, 28% PEG MME 550) were mixed and equilibrated against reservoir solution (500 µl) at 289 K. Crystals formed within 4 d and grew to maximum dimensions of 0.1 × 0.1 × 0.1 mm.

2.2. Data collection and processing

Diffraction data were collected on the BL13B1 beamline at the National Synchrotron Radiation Research Center (NSRRC), Hsinchu, Taiwan and at the Macromolecular X-ray Crystallographic Center of the NTHU Instrument Center at National Tsing Hua University, Hsinchu, Taiwan. Crystals were mounted from the mother liquor on nylon loops and were immediately flash-cooled by submersion in liquid

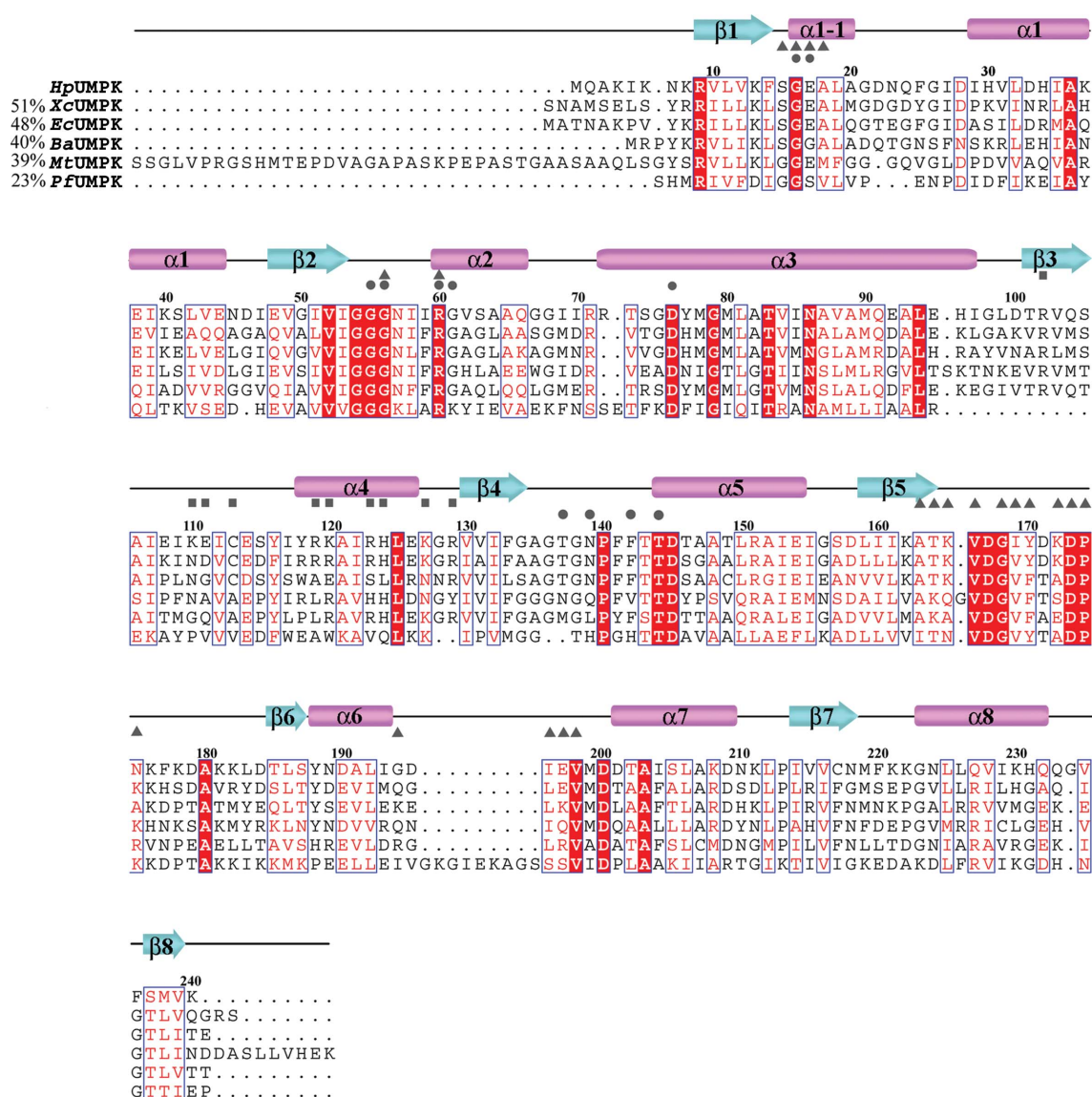


Figure 1

Sequence alignment of UMPKs from *Helicobacter pylori* 26695 (*Hp*UMP_K), *Xanthomonas campestris* (*Xc*UMP_K), *Escherichia coli* (*Ec*UMP_K), *Bacillus anthracis* (*Ba*UMP_K), *Mycobacterium tuberculosis* (*Mt*UMP_K) and *Pyrococcus furiosus* (*Pf*UMP_K). The alignment was performed by *ClustalW* (Thompson *et al.*, 1994). The percentage of identical residues for each species relative to *Hp*UMP_K is shown to the left of each sequence. Completely conserved residues are shown on a red background and conservatively exchanged residues are shown in red. The numbering is that of the *Hp*UMP_K sequence. Secondary-structure elements of *Hp*UMP_K are shown as cyan arrows for β -strands and as pink cylinders for α -helices. *Pf*UMP_K residues that interact with AMPPNP are marked by triangles. *Hp*UMP_K residues that interact with GTP and UDP are marked by squares and circles, respectively.

nitrogen. *Hp*UMP K –GTP data were collected to 1.8 Å resolution using a wavelength of 1.000 Å and *Hp*UMP K –UDP data were collected to 2.5 Å resolution using a wavelength of 0.979 Å. The data sets were indexed, integrated and scaled using *HKL*-2000 (Otwinowski & Minor, 1997). The *Hp*UMP K –GTP crystal belonged to the primitive rhombohedral space group *R*32 and had unit-cell parameters $a = b = 137.4$, $c = 152.9$ Å in the hexagonal lattice. R_{merge} was 6.7%. The Matthews coefficient (V_M ; Matthews, 1968) was calculated as 2.65 Å³ Da^{−1}, which corresponded to a solvent content of 54% for two protomers per asymmetric unit. The *Hp*UMP K –UDP crystal belonged to the monoclinic space group *C*2 and had unit-cell parameters $a = 147.1$, $b = 127.6$, $c = 93.2$ Å, $\beta = 91.5^\circ$. R_{merge} was 5.7%. V_M (Matthews, 1968) was calculated as 2.78 Å³ Da^{−1}, which corresponded to a solvent content of 44% for six protomers per asymmetric unit. Detailed data statistics are summarized in Table 1.

2.3. Structure determination and refinement

The structures of *Hp*UMP K –UDP and *Hp*UMP K –GTP were solved by molecular replacement using *MOLREP* (Vagin & Teplyakov, 2010) with the crystal structures of *Ec*UMP K (PDB entry 2bnd; Briozzo *et al.*, 2005) and *Hp*UMP K –UDP (PDB entry 4a7x; this work), respectively, as search models. Model building used *Coot* (Emsley & Cowtan, 2004) and refinement used *REFMAC5* (Murshudov *et al.*, 2011) and *PHENIX* (Terwilliger *et al.*, 2008). Noncrystallographic symmetry (NCS) restraints were not applied for either *Hp*UMP K –GTP or *Hp*UMP K –UDP during restrained

refinement. The final model of *Hp*UMP K –GTP with two protomers per asymmetric unit contained 3428 protein atoms, 316 waters, two glycerol molecules and two GTP molecules, with an *R* factor of 19.0% and an R_{free} of 22.7%. The final model of *Hp*UMP K –UDP with six protomers per asymmetric unit contained 10 464 protein atoms, 393 waters and four UDP molecules, with an *R* factor of 21.6% and an R_{free} of 27.6%. The geometric quality of the structures was assessed using Ramachandran plots generated by *MolProbity* (Chen *et al.*, 2010; Davis *et al.*, 2007). Detailed refinement statistics are summarized in Table 1. The data completeness and *R* values of *Hp*UMP K –UDP differed from those in the EDS (Uppsala Electron Density Server) summary because reflections with F_{obs} equal to or less than zero are removed in the EDS. Atomic coordinates for *Hp*UMP K –GTP and *Hp*UMP K –UDP were deposited in the Protein Data Bank (PDB entries 4a7w and 4a7x, respectively).

3. Results and discussion

3.1. Multiple sequence alignment

The aligned sequences of UMPKs from *H. pylori*, the Gram-negative bacteria *Xanthomonas campestris* (*Xc*UMP K ; Tu *et al.*, 2009) and *E. coli* (*Ec*UMP K ; Briozzo *et al.*, 2005), the Gram-positive bacteria *B. anthracis* (Meier *et al.*, 2008) and *Mycobacterium tuberculosis* (Labesse *et al.*, 2011) and the archaeon *Pyrococcus furiosus* (*Pf*UMP K ; Marco-Marín, Escamilla-Honrubia *et al.*, 2005) are shown in Fig. 1. *Hp*UMP K shares a sequence identity of between 23 and 51%

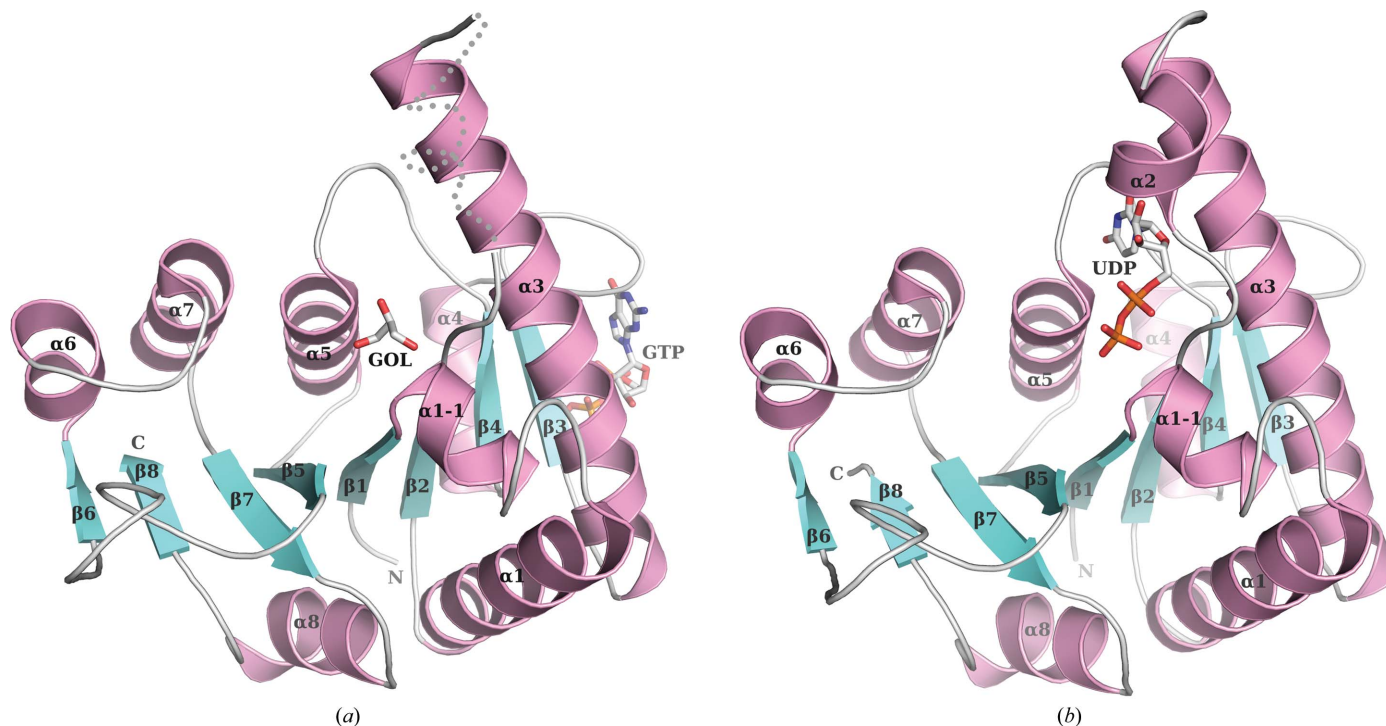


Figure 2
*Hp*UMP K –GTP and *Hp*UMP K –UDP monomeric structures: ribbon representations of (a) *Hp*UMP K –GTP and (b) *Hp*UMP K –UDP monomers. The α -helices are coloured pink and the β -strands are coloured cyan. Electron density was not found for $\alpha 2$ (Arg60–Gly68) in *Hp*UMP K –GTP and this sequence is marked as a dashed line in (a). GTP and glycerol are shown as ball-and-stick models in (a). UDP is shown as a ball-and-stick model in (b).

with these UMPKs; however, its sequence is only 8.9% identical to that of human UMP/CMP kinase (Segura-Peña *et al.*, 2004; data not shown). Using the *Pf*UMPK–adenylyl-imidodiphosphate (AMPPNP) structure as a guide (Marco-Marín, Escamilla-Honrubia *et al.*, 2005), it appears that many of the ATP-binding residues are probably conserved in the UMPK sequences shown in Fig. 1, including Gly16, Gly56, Arg60, Val166, Gly168, Asp173, Pro174 and Val198 (*Hp*UMPK sequence numbering). However, two other ATP-binding residues in *Pf*UMPK, corresponding to Thr164 and Tyr170 in *Hp*UMPK, are only also found in the *Hp*UMPK sequence. Examination of the *Ec*UMPK–UNP structure (Briozzo *et al.*, 2005) indicates that the UNP-binding residues Lys13, Ser15, Gly16, Gly55, Gly56, Arg60, Gly61, Asp76, Thr137, Asn13 and Thr144 (*Hp*UMPK sequence numbering) are also highly conserved in Gram-negative bacterial UMPK sequences. Comparison of the GTP-binding residues between *Ec*UMPK–GTP (Meyer *et al.*, 2008) and *Xc*UMPK–GTP (Tu *et al.*, 2009) indicates that these residues are found around loop $\alpha 3\beta 3$, $\alpha 4$ and loop $\alpha 4\beta 4$. However, the difference is that in *Ec*UMPK–GTP three residues are located in $\alpha 3$; in contrast, in *Xc*UMPK–GTP one residue is located in $\beta 3$. Moreover, among the ATP-, UNP- and GTP-binding residues of UMPKs, the latter binding residues are considerably diverse.

3.2. *Hp*UMPK–GTP and *Hp*UMPK–UDP structures

The *Hp*UMPK–GTP and *Hp*UMPK–UDP monomers both contain an α/β -fold, with the eight-stranded β -sheet sandwiched between $\alpha 1$, $\alpha 1-1$, $\alpha 2$, $\alpha 3$ and $\alpha 8$ on one side and $\alpha 4$,

$\alpha 5$, $\alpha 6$ and $\alpha 7$ on the other (Fig. 2). The central β -sheet consists of eight β -strands, including six parallel β -strands ($\beta 3$, $\beta 4$, $\beta 2$, $\beta 1$, $\beta 5$ and $\beta 7$) and two additional parallel β -strands ($\beta 8$ and $\beta 6$) in the opposite direction (Fig. 2). In *Hp*UMPK–GTP the GTP molecule is found on the surface of the *Hp*UMPK monomer near loop $\beta 3\alpha 4$ (Fig. 2*a*). In *Hp*UMPK–UDP the UDP molecule is surrounded by $\alpha 1-1$, $\alpha 2$, $\alpha 3$ and $\alpha 5$ (Fig. 2*b*). The root-mean-square deviation (r.m.s.d.) for the *Hp*UMPK–GTP and *Hp*UMPK–UDP C α atoms is 0.27 Å. The overall folds of the ligand-free and ligand-bound states are similar in *Hp*UMPK and are also similar to those in bacterial UMPKs (Labesse *et al.*, 2011; Tu *et al.*, 2009; Meier *et al.*, 2008). It should be mentioned that the $\alpha 2$ helix is well defined in *Hp*UMPK–UDP (Fig. 2*b*); however, electron density for $\alpha 2$ is missing in *Hp*UMPK–GTP (Fig. 2*a*).

The two protomers of *Hp*UMPK–GTP, *A* and *B* (Fig. 3*a*), are related by a noncrystallographic twofold axis with 42% of the peak height of the real twofold axis in the self-rotation function as calculated using the program *GLRF* (Tong & Rossmann, 1997). The r.m.s.d. for all C α atoms between the two protomers was calculated as 0.07 Å. As expected, *Hp*UMPK–GTP packs as a hexamer and can be thought of as a well packed set of three dimers, *AB*, *A'B'* and *A''B''*, or as a set of two trimers, *AA'A''* and *BB'B''* (where the primes denote symmetry-related molecules). Six GTPs are found per *Hp*UMPK–GTP hexamer, with the GTPs at the centre of the hexamer. Therefore, GTP possibly assists in hexamer formation and stability. Conversely, in *Hp*UMPK–UDP the six protomers (labelled *A*, *B*, *C*, *D*, *E* and *F*) are loosely packed as an asymmetric hexamer (Fig. 3*b*) and UDP is only observed in

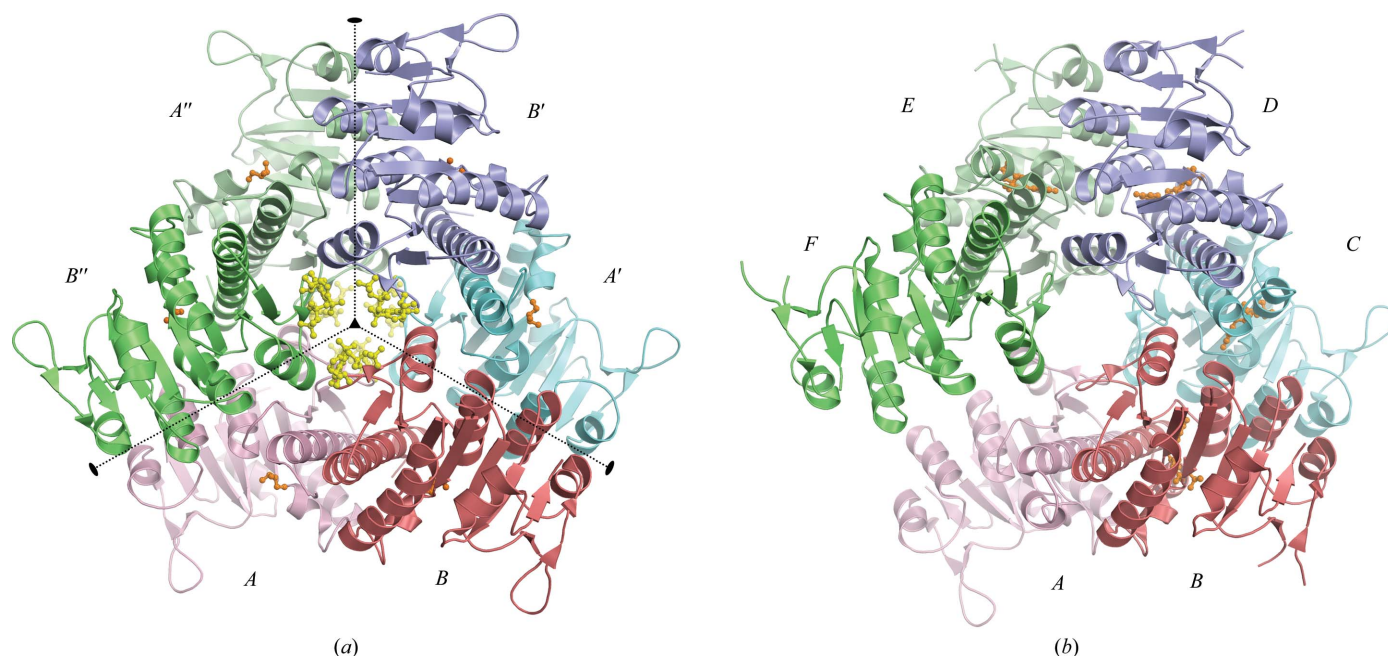


Figure 3

*Hp*UMPK–GTP and *Hp*UMPK–UDP quaternary structures. (a) A ribbon diagram of the *Hp*UMPK–GTP hexamer viewed along the threefold crystallographic axis (indicated by the triangle). The three noncrystallographic twofold axes are shown as dotted lines; the two molecules in the asymmetric units are coloured pink and salmon (*A* and *B*), cyan and purple (*A'* and *B'*) and light green and green (*A''* and *B''*). GTP and glycerol are coloured yellow and orange, respectively, and are shown as ball-and-stick models. (b) A ribbon diagram of *Hp*UMPK–UDP. The six molecules of the asymmetric unit are coloured pink, salmon, cyan, purple, light green and green and are labelled *A*, *B*, *C*, *D*, *E* and *F*. UDP is shown as an orange ball-and-stick model.

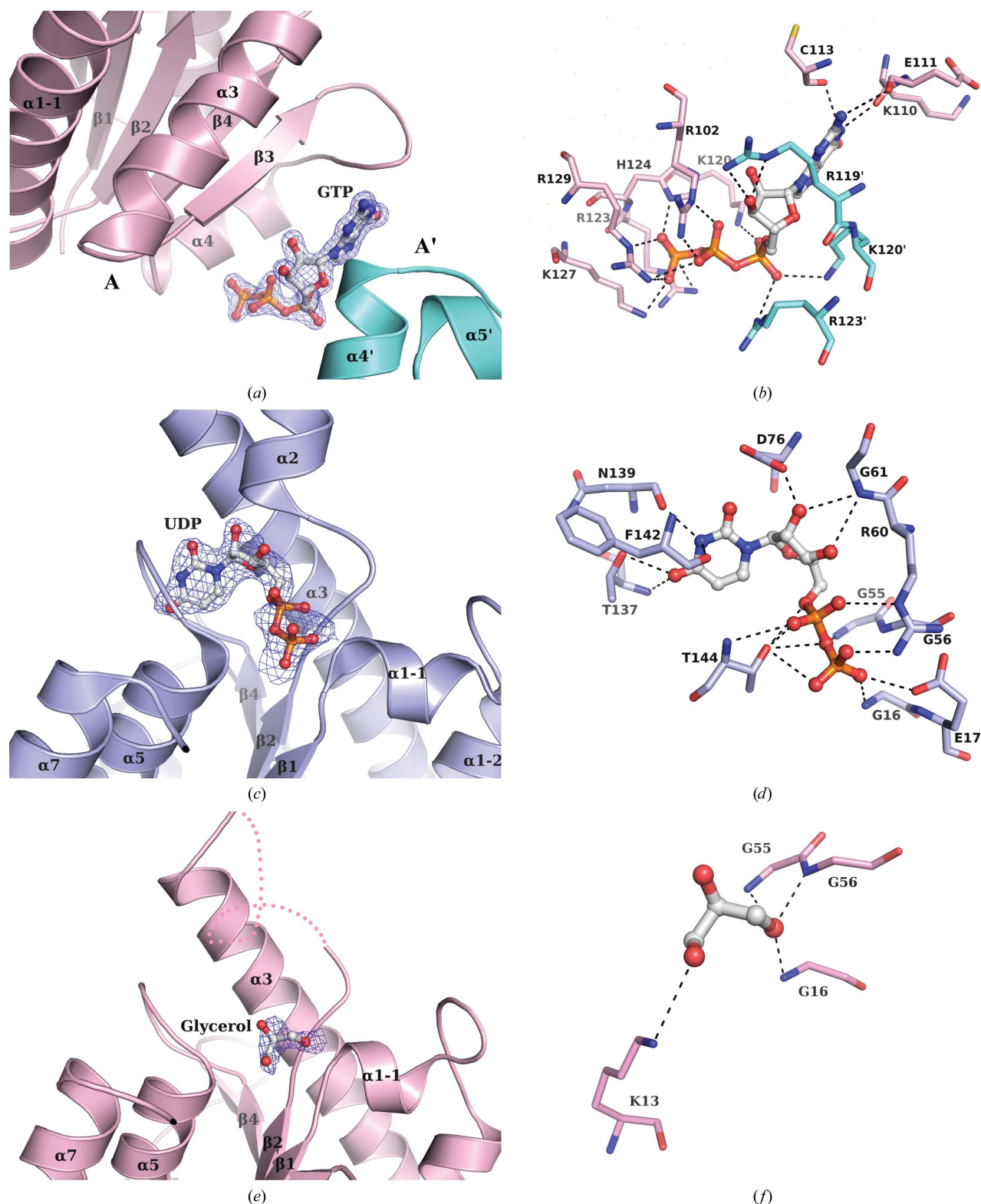


Figure 4

Nucleotide-binding sites in *HpUMPk*-GTP and *HpUMPk*-UDP. (a) The GTP-binding site in *HpUMPk*-GTP. A ribbon representation of the interdimers subunits (e.g. A and A', coloured pink and cyan, respectively) involved in GTP binding. The $mF_o - DF_c$ map of GTP in *HpUMPk*-GTP is contoured at 3.0σ , with GTP shown as a ball-and-stick model. Numerically identical residues with and without primes belong to neighbouring subunits. (b) The *HpUMPk* GTP-binding residues are shown as stick models. GTP is shown as a ball-and-stick model. (c) The UDP-binding site in *HpUMPk*-UDP. The $mF_o - DF_c$ map for UDP in *HpUMPk*-UDP is contoured at 3.0σ . UDP is drawn as a ball-and-stick model. (d) The UDP-binding residues of *HpUMPk*-UDP are shown as stick models. UDP is drawn as a ball-and-stick model. (e) The *HpUMPk*-GTP glycerol-binding site. The glycerol $mF_o - DF_c$ map in *HpUMPk*-GTP is contoured at 3.0σ . (f) The *HpUMPk* residues that interact with glycerol are shown as stick models. Glycerol is drawn as a ball-and-stick model. Hydrogen bonds are shown as black dashed lines in (b), (d) and (f).

protomers *B*, *C*, *D* and *E*. Therefore, the hexameric symmetry found for *Ec*UMPK–UDP, in which each subunit contains a UDP (Briozzo *et al.*, 2005), is not observed in *Hp*UMPK–UDP (Fig. 3*b*). Because UDP is the product of UMP phosphorylation, the binding affinity between UDP and UMPK should be relatively weak. In addition, the UDP concentration in the crystallization medium was 1 mM, which is a lower concentration than that used in the crystallization of *Ec*UMPK–UDP (50 mM; Briozzo *et al.*, 2005) and may also explain why *Hp*UMPK–UDP contains only four UDPs per hexamer. For *Hp*UMPK–UDP the two protomers in the *AB*, *CD* and *EF* dimers are related by noncrystallographic twofold axes (25–40% of the peak height of the real twofold axis in the self-rotation function). These three dimers form the asymmetric hexamer *via* a noncrystallographic threefold axis (38% of the peak height of the real twofold axis in the self-rotation function). The elastic alteration of the asymmetric hexamer in the *Hp*UMPK–UDP oligomer may assist in the release of UDP, as in the UDP-free form of protomers *A* and *F* in *Hp*UMPK–UDP.

3.3. Nucleotide-binding sites in *Hp*UMPK–GTP and *Hp*UMPK–UDP

For *Hp*UMPK–GTP, the GTP positions were found in the $mF_o - F_c$ map at 3.0σ and GTP is situated between the $\alpha 4$ and $\alpha 4'$ helices of two different subunits (*A* and *A'*; Figs. 3*a* and 4*a*). Interactions between the GTP phosphate O atoms and the side chains of Arg102, His124, Lys127 and Arg129 are mainly responsible for binding (Fig. 4*b*, Table 2). The extremely basic environment is appropriate for GTP phosphate binding. The guanine atoms hydrogen bond to the residues Lys110, Glu111 and Cys113 in loop $\beta 3\alpha 4$ (Fig. 4*b*). Additionally, the side chains of Arg119', Lys120' and Arg123' in the adjacent subunit interact with the ribose O3' and the α -phosphate O atom (Fig. 4*b*). *Hp*UMPK–GTP, *Xc*UMPK–GTP (Tu *et al.*, 2009) and *Ec*UMPK–GTP (Meyer *et al.*, 2008) are the three GTP-complex structures of UMPK from Gram-negative bacteria that are available in the PDB to date. The GTP-binding sites of *Hp*UMPK and *Xc*UMPK (Tu *et al.*, 2009) are located at the centre of the hexamer. Of the ten GTP-binding residues in *Hp*UMPK, five residues, Arg102, Arg119, Arg123, Lys127 and Arg129, are identical to those in *Xc*UMPK (Fig. 1). In contrast, GTP binds at the dimeric interface of *Ec*UMPK and its position and the GTP-binding residues differ from those observed in the *Hp*UMPK and *Xc*UMPK complexes.

*Hp*UMPK–UDP is an unusual hexameric UMPK structure in that (as noted above) it is not a symmetrical structure (Fig. 3*b*). The $mF_o - DF_c$ map for UDP in *Hp*UMPK–UDP is shown contoured at 3.0σ in Fig. 4(*c*). UDP is located near $\alpha 1$ -1, $\alpha 2$, $\alpha 3$ and $\alpha 5$ and the C-termini of $\beta 1$, $\beta 2$ and $\beta 4$ (Figs. 2*b* and 4*c*). The UDP-binding site of *Hp*UMPK is similar to those of other UMPKs. The interactions between UDP and protomers *B*, *C*, *D* and *E* differ slightly, and protomer *D* possesses the most interactions with UDP (Fig. 4*d*). The UDP phosphate O atoms interact with Gly16, Glu17, Gly55, Gly56,

Table 2

Hydrogen bonds between *Hp*UMPK and the ligands GTP, UDP and glycerol.

Ligand (atom)	Residue (atom)	Distance (Å)
GTP		
N1	Lys110 O	2.7
	Cys113 O	3.1
N2	Lys110 O	3.0
O3'	Arg119' NE	2.9
	Arg119' NH2	3.0
O1 α	Lys120 NZ	3.1
O1 β	Arg102 NH2	2.7
	Arg129 NH2	3.2
O2 α	Lys120' NZ	3.1
	Arg123' NH2	3.1
O2 β	Arg102 NE	2.7
O2 γ	His124 ND1	2.6
	Arg129 NE	2.7
O3 γ	Lys127 NZ	2.7
	Arg129 NH2	3.0
UDP		
N3	Asn139 O	2.8
	Phe142 O	2.9
O3	Thr144 OG1	3.1
O4	Thr137 N	2.9
	Thr137 OG1	3.0
O2'	Gly61 N	3.2
	Asp76 OD1	2.4
O3'	Gly61 N	3.4
O5'	Thr144 OG1	3.2
	Thr144 OG1	2.6
O1 α	Thr144 N	3.4
O1 β	Arg60 NH2	2.6
	Arg60 NE	3.4
O2 α	Gly16 N	2.6
O2 β	Glu17 OE1	3.0
	Gly55 N	3.2
O3 α	Thr144 OG1	3.4
O3 β		
Glycerol		
O1	Gly16 N	2.6
	Gly55 N	3.3
	Gly56 N	2.8
O3	Lys13 NZ	3.0

Arg60 and Thr144 from $\alpha 1$ -1, loop $\beta 2\alpha 2$, $\alpha 2$ and $\alpha 5$ (Table 2). The UDP uracil interacts with residues Thr137, Asn139 and Phe142 in loop $\beta 4\alpha 5$ and the UDP ribose interacts with Gly61 from $\alpha 2$, Asp76 from $\alpha 3$ and Thr144 from $\alpha 5$. Most of the aforementioned UDP-binding residues are conserved in UMPKs, with the exceptions of Thr137, Asn139 and Phe142, which are only found in Gram-negative bacterial UMPKs.

Electron density for $\alpha 2$ and loop $\alpha 2\alpha 3$ (Arg60–Gly68; UDP-binding region) is well defined in *Hp*UMPK–UDP but is not observed in *Hp*UMPK–GTP because of the consequences of UDP binding. UDP binding appears to stabilize the conformation of $\alpha 2$ and loop $\alpha 2\alpha 3$ in the *Hp*UMPK–UDP complex. The *Hp*UMPK–GTP crystal was obtained in a crystallization medium that contained both GTP and UDP. However, only GTP binds to *Hp*UMPK, and six GTP molecules were determined in the *Hp*UMPK–GTP hexamer. It might be proposed that *Hp*UMPK favours GTP binding over UDP binding under these particular conditions. In the *Mt*UMPK–GTP/UDP complex (Labesse *et al.*, 2011), which is a hexameric complex, one promoter contains both GTP and UDP and the other five protomers have GTP but not UDP bound. The $\alpha 2$ helices of all six protomers are well observed. From further soaking

experiments, *Mt*UMPK appears to be unable to bind six UMP molecules completely. This suggests that binding between GTP and UDP might exist in a dynamic equilibrium that may be related to the enzymatic function of UMPK. The activity of UMPK can be increased by GTP, which is an allosteric activator (Serina *et al.*, 1996); thus, GTP binding may promote the release of the product UDP in order to facilitate ATP-dependent phosphorylation.

However, electron density is present within the UDP-binding site in the *Hp*UMPK–GTP $mF_o - DF_c$ map, but only at the UDP β -phosphate position (Figs. 4e and 2a). Of the various possible molecules/ions that might be responsible for this extra density, the density could only be fitted by a glycerol molecule (B factor = 26.7 \AA^2). The glycerol molecule forms hydrogen bonds to Lys13, Gly16, Glu17, Gly56 and Thr144

(Table 2), all of which, apart from Lys13, interact with UDP in *Hp*UMPK–UDP (Fig. 4f).

3.4. Molecular motions within the *Hp*UMPK hexamer

The interfaces of the *Hp*UMPK–GTP hexamer involve two types of dimers: an intradimer (AB) and an interdimer (BA'), which have buried surface areas of 1301.27 and 965.57 \AA^2 , respectively (Fig. 3a). Hydrophobic interactions involving the side chains of Met78, Leu81, Val84, Ile85, Val88 and Ala89 in $\alpha 3$ and $\alpha 3'$ appear to stabilize the intradimer interface (Fig. 5a). These interactions are observed at the *Hp*UMPK–UDP AB , CD and EF interfaces (protomers B , C , D and E are UDP-bound forms), as well as the *Hp*UMPK–GTP AB interface. These hydrophobic residues are conserved in the sequences of the bacterial UMPKs shown in Fig. 1.

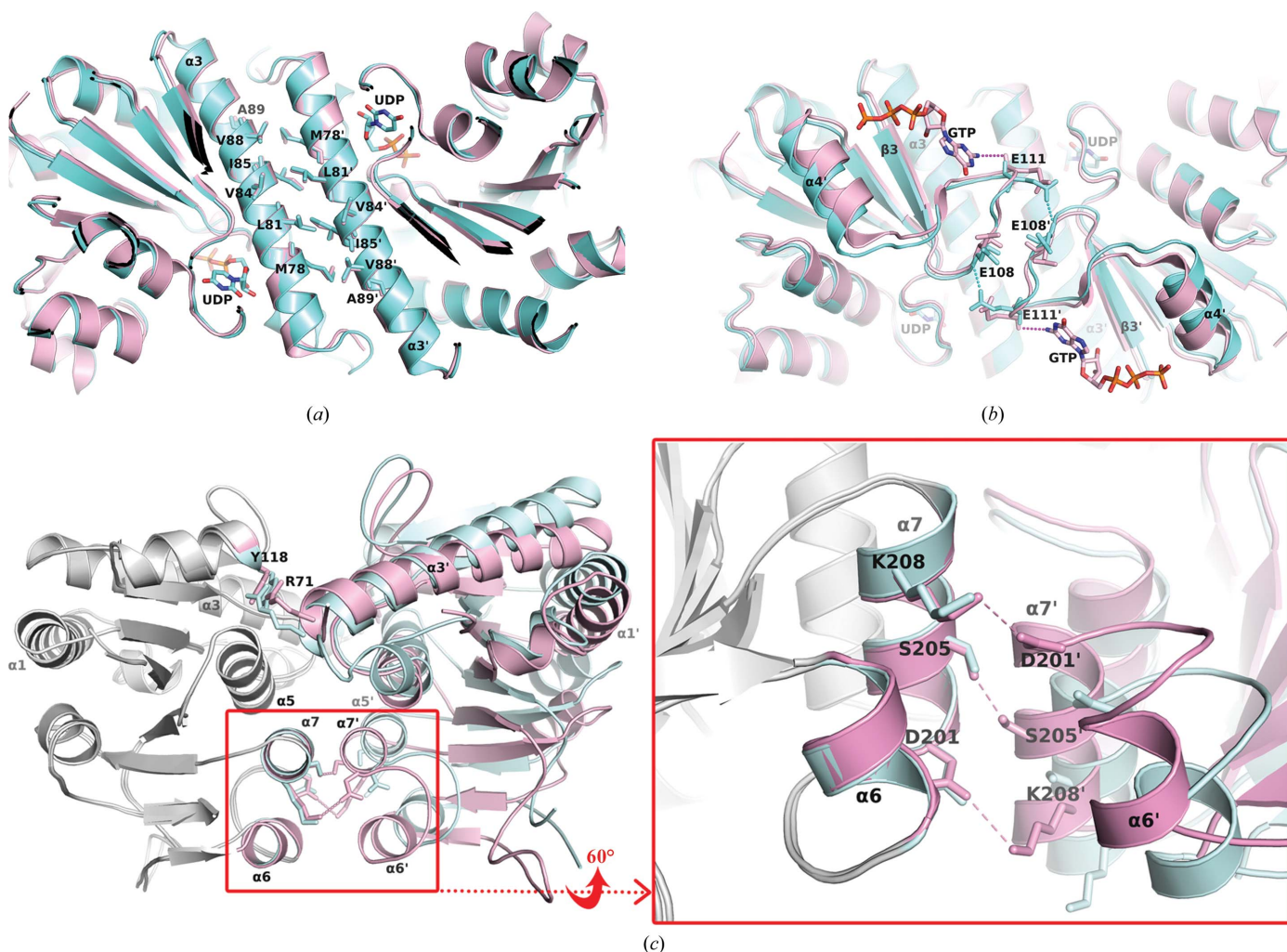


Figure 5

Molecular motions within the *Hp*UMPK hexamer. (a, b) Ribbon diagrams showing superposition of the AB dimer from *Hp*UMPK–GTP (pink) and the CD dimer from *Hp*UMPK–UDP (cyan). (a) Hydrophobic interactions at the interface of AB and CD . UDP molecules are shown as cyan stick models. The hydrophobic residues Met78, Leu81, Val84, Ile85, Val88 and Ala89 from the $\alpha 3$ and $\alpha 3'$ helices that interact are shown as stick models. (b) Hydrophilic interactions between subunits AB and CD . GTP molecules are shown as pink stick models. Glu111 and Glu108 from loop $\beta 3\alpha 4$ are shown as stick models and hydrogen bonds are shown as dashed lines. (c) Superpositioned ribbon diagrams of the *Hp*UMPK–GTP A' and B subunits (A' , grey; B , pink) and the *Hp*UMPK–UDP C and B subunits (C , grey; B , cyan). In the left panel, the superpositioning of the subunits on the left emphasizes the rotation of the subunits on the right by $\sim 11^\circ$. The right panel shows an enlargement of the red box in the left panel rotated around the y axis by $\sim 60^\circ$ to emphasize the interactions between $\alpha 7$ and $\alpha 7'$. Asp201, Ser205, and Lys208 are shown as stick models. Hydrogen bonds are shown as dashed lines.

Additionally, a unique hydrophilic interaction is observed at the *Hp*UMP K –UDP CD intradimer interface in which the loop $\beta 3\alpha 4$ residues Glu108 and Glu111 from neighbouring protomers form hydrogen bonds. Glu108 and Glu111 are not found in the sequences of the other UMP K s shown in Fig. 1. Notably, an analogous hydrogen bond is formed in *Urea-plasma parvum* UMP K by Lys102 and Cys103 from neighbouring subunits at the intradimer interface (Egeblad-Welin *et al.*, 2007).

As in *Xc*UMP K (Tu *et al.*, 2009), the *Hp*UMP K loop $\beta 3\alpha 4$ residues (Ala106–Ile117) participate in GTP binding. Loop $\beta 3\alpha 4$ is longer than the corresponding loop in *Pf*UMP K (Fig. 1), which precludes GTP binding and thereby prevents activation by GTP (Egeblad-Welin *et al.*, 2007; Jensen *et al.*, 2007). Interestingly, the hydrogen bonds between Glu108 and Glu111 from neighbouring protomers are absent in *Hp*UMP K –GTP; instead, the backbone amide of Glu111 hydrogen bonds to N2 of the GTP guanine (Fig. 5*b*), as do Lys110 and Cys113 from loop $\beta 3\alpha 4$ (Table 2). In summary, residues in $\beta 3$, loop $\beta 3\alpha 4$ and $\alpha 4$ bind GTP in bacterial UMP K s (Labesse *et al.*, 2011; Tu *et al.*, 2009; Meyer *et al.*, 2008). Our studies demonstrate that loop $\beta 3\alpha 4$ in *Hp*UMP K is responsible for intradimer interactions and for GTP binding.

The interface of the interdimer (BA') resides between the two trimers ($AA'A''$ and $BB'B''$; Fig. 3*a*). A superposition of the *Hp*UMP K –GTP BA' dimer and the *Hp*UMP K –UDP BC dimer is shown in Fig. 5(*c*) and the r.m.s.d. for the C^α atoms of

the two dimers is 0.363 Å. In *Hp*UMP K –GTP the interdimer interface is mainly formed by $\alpha 7$ and $\alpha 7'$, with the intersubunit interactions involving salt bridges between Asp201 and Lys208 and a hydrogen bond between the two complementary Ser205 residues (Fig. 5*c*). Although the $\alpha 7$ helices pack tightly against each other in *Hp*UMP K –GTP, they are well separated in *Hp*UMP K –UDP (the distance between the Ser205 C^α atoms in the subunits is 12.5 Å). As a result, *Hp*UMP K –GTP is more stable (resolution 1.8 Å, average B factor 25.2 Å²) than *Hp*UMP K –UDP (resolution 2.5 Å, average B factor 51.4 Å²). Asp201, Ser205 and Lys208 are not conserved among the UMP K sequences shown in Fig. 1, suggesting that their interactions are unique to *Hp*UMP K –GTP.

In addition, a hydrogen-bond or salt-bridge interaction between $\alpha 3$ and $\alpha 4$ from the interdimer subunits is found in UMP K s, such as a hydrogen bond between Arg71 in loop $\alpha 2\alpha 3$ and Tyr118 in $\alpha 4$ in *Hp*UMP K and a salt bridge between Asn72 (in loop $\alpha 2\alpha 3$) and Glu157 (in $\alpha 5$) in *Ec*UMP K (Fig. 1; Tu *et al.*, 2009; Meyer *et al.*, 2008; Meier *et al.*, 2008; Marco-Marín, Gil-Ortiz *et al.*, 2005). GTP binding rotates the interdimer subunits by $\sim 11^\circ$ (Meyer *et al.*, 2008). This rotation tightens the interdimer interface, whereas the intradimer interface is loose. Interestingly, the Arg71–Tyr118 hydrogen bond is present, as is the 11° rotation of protomer B (the positions of protomers A' and C are fixed), in *Hp*UMP K –GTP and *Hp*UMP K –UDP. The molecular movements within the *Hp*UMP K hexamer induced by GTP or UDP may therefore affect UMP K catalysis. It is also possible that the GTP-induced interactions made by Asp201, Ser205 and Lys208 in $\alpha 7$ of *Hp*UMP K –GTP are necessary for perfect hexameric symmetry. On the other hand, this molecular movement causes asymmetric assembly of the subunits in *Hp*UMP K –UDP.

3.5. The ATP-, UNP- and GTP-binding sites in *Hp*UMP K

Given their catalytic and allosteric mechanisms and previous structural reports (Marco-Marín, Gil-Ortiz *et al.*, 2005; Jensen *et al.*, 2007; Meyer *et al.*, 2008; Tu *et al.*, 2009), bacterial UMP K s contain three binding sites (ATP-, GTP- and UNP-binding sites). We identified the GTP- and UDP-binding sites in *Hp*UMP K ; however, the ATP-binding site was not characterized. To date, only two UMP K –ATP or ATP-analogue complexes have been reported: from *P. furiosus* (Marco-Marín, Gil-Ortiz *et al.*, 2005) and *Sulfolobus solfataricus* (Jensen *et al.*, 2007).

Superpositioned *Hp*UMP K –GTP, *Hp*UMP K –UDP and *Pf*UMP K –AMPPNP/UMP monomers are shown in Fig. 6. Although *Hp*UMP K and *Pf*UMP K share only 23% sequence identity (Fig. 1), their overall structures are similar, with an r.m.s.d. for C^α atoms of 1.4 Å. The UMP-binding site in *Pf*UMP K and the UDP-binding site in *Hp*UMP K are found in similar positions. The AMPPNP-binding site in *Pf*UMP K appears to also exist in *Hp*UMP K , *i.e.* a groove delineated by $\beta 1$, $\beta 5$, $\beta 6$, $\beta 7$ and $\beta 8$ and loops $\beta 5\beta 6$ and $\alpha 6\alpha 7$ (Figs. 2 and 6). The UDP-binding and proposed ATP-binding sites in *Hp*UMP K form a continuous groove such that the

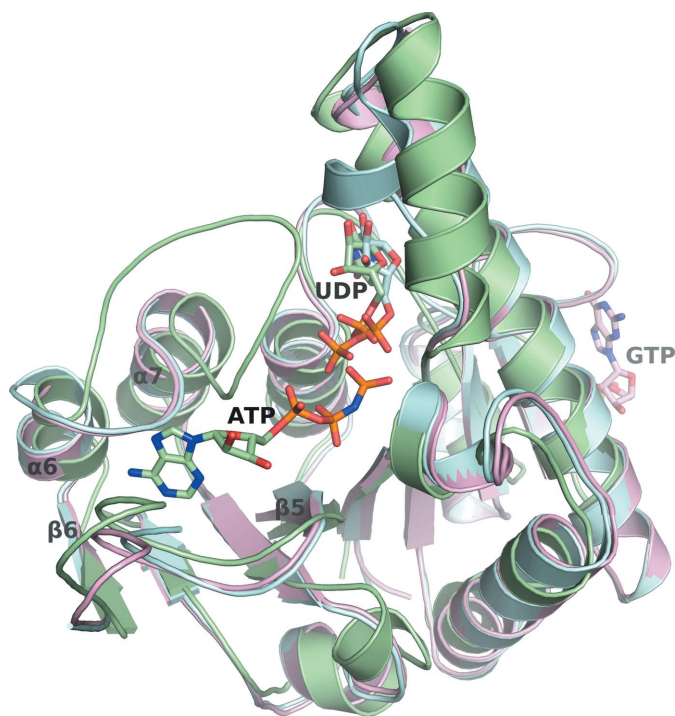


Figure 6

Superpositioned *Hp*UMP K –GTP, *Hp*UMP K –UDP and *Pf*UMP K –AMPPNP/UMP monomers. *Hp*UMP K –GTP, *Hp*UMP K –UDP and *Pf*UMP K –AMPPNP/UMP (PDB entry 2bmu; Marco-Marín, Gil-Ortiz *et al.*, 2005) are shown as ribbon diagrams and coloured pink, cyan and green, respectively. GTP, UDP, UMP and AMPPNP are shown as stick models and coloured the same as their associated UMP K s.

γ -phosphate of ATP and the β -phosphate of UDP would be separated by 2.8 Å. This positioning of the terminal ATP and UMP phosphates would facilitate the transfer of the γ -phosphate of ATP to UMP. In *Pf*UMPCK, AMPNP is sandwiched between loops $\beta 5\beta 6$ and $\alpha F\alpha G$ (Marco-Marín, Gil-Ortiz *et al.*, 2005). The corresponding loops in *Hp*UMPCK are loops $\beta 5\beta 6$ and $\alpha 6\alpha 7$ (Fig. 6). Loop $\alpha 6\alpha 7$ in *Hp*UMPCK (seven residues) is shorter than loop $\alpha F\alpha G$ in *Pf*UMPCK, which contains 16 residues. The corresponding loops in the other bacterial UMPCK sequences (Fig. 1) also contain only seven residues, suggesting that the ATP-binding mode in bacterial UMPCKs might not resemble that in archaeal UMPCKs.

For *Hp*UMPCK, the binding site of GTP is well separated from the ATP-binding and proposed UDP-binding sites (~ 21 Å for GTP C1' and the UDP β -phosphate and ~ 27 Å for GTP C1' and the ATP γ -phosphate). In *Hp*UMPCK-UDP $\alpha 2$ and loop $\alpha 2\alpha 3$ have an average B factor of 56.2 Å^2 ; in contrast, the average B factor for the UDP-free protomers of *Hp*UMPCK-UDP was 83.0 Å^2 , indicating high flexibility. Furthermore, electron density for this region is missing in *Hp*UMPCK-GTP. $\alpha 2$ and loop $\alpha 2\alpha 3$ maintain stable conformations when UDP is bound, whereas they become too flexible to be observed when UDP is absent in *Hp*UMPCK-GTP. This suggests that GTP, which is an allosteric active effector, may regulate the conformation of $\alpha 2$ and loop $\alpha 2\alpha 3$ to promote UDP release. Consequently, the conformations of $\alpha 2$ and loop $\alpha 2\alpha 3$ could be important for substrate (UMP) binding and product (UDP) release.

Given the structures of *Hp*UMPCK-GTP and *Hp*UMPCK-UDP, we can propose a mechanism for UDP release. When GTP binds to *Hp*UMPCK, *Hp*UMPCK-GTP forms a compact, tight and stable hexameric conformation, and it may be not easy to release the product UDP from such a stable oligomerization state. However, UDP could be promoted for release through triggering a conformational change of the UDP-binding region ($\alpha 2$) to loosen its firmness. Therefore, GTP binding may induce a conformation of $\alpha 2$ that assists UDP release through an allosteric effect; however, further studies are needed in order to conclusively demonstrate these hypotheses. Nevertheless, when GTP is absent the typical hexameric symmetry of UMPCK is destroyed, as observed in *Hp*UMPCK-UDP; the interface of the dimer is exposed and may facilitate UDP release in the absence of steric interference.

This work was supported by grants from the National Science Council of Taiwan, Republic of China (NSC 99-2311-B-007-007 to Y-JS) and the National Tsing Hua University, Taiwan, Republic of China (100N2715E1 to Y-JS). We are grateful for access to the BL13B1 beamline at the National Synchrotron Radiation Research Center in Hsinchu, Taiwan and the Macromolecular X-ray Crystallographic Center of the NTHU Instrument Center at National Tsing Hua University, Hsinchu, Taiwan, Republic of China.

References

- Akerley, B. J., Rubin, E. J., Novick, V. L., Amaya, K., Judson, N. & Mekalanos, J. J. (2002). *Proc. Natl Acad. Sci. USA*, **99**, 966–971.
- Briozzo, P., Evrin, C., Meyer, P., Assairi, L., Joly, N., Barzu, O. & Gilles, A. M. (2005). *J. Biol. Chem.* **280**, 25533–25540.
- Chen, V. B., Arendall, W. B., Headd, J. J., Keedy, D. A., Immormino, R. M., Kapral, G. J., Murray, L. W., Richardson, J. S. & Richardson, D. C. (2010). *Acta Cryst.* **D66**, 12–21.
- Davis, I. W., Leaver-Fay, A., Chen, V. B., Block, J. N., Kapral, G. J., Wang, X., Murray, L. W., Arendall, W. B., Snoeyink, J., Richardson, J. S. & Richardson, D. C. (2007). *Nucleic Acids Res.* **35**, W375–383.
- Egeblad-Welin, L., Welin, M., Wang, L. & Eriksson, S. (2007). *FEBS J.* **274**, 6403–6414.
- Emsley, P. & Cowtan, K. (2004). *Acta Cryst.* **D60**, 2126–2132.
- Fassy, F., Krebs, O., Lowinski, M., Ferrari, P., Winter, J., Collard-Dutilleul, V. & Salahbey Hocini, K. (2004). *Biochem. J.* **384**, 619–627.
- Gagyi, C., Bucurenci, N., Sirbu, O., Labesse, G., Ionescu, M., Ofiteru, A., Assairi, L., Landais, S., Danchin, A., Bârz, O. & Gilles, A. M. (2003). *Eur. J. Biochem.* **270**, 3196–3204.
- Humeniuk, R., Menon, L. G., Mishra, P. J., Gorlick, R., Sowers, R., Rode, W., Pizzorno, G., Cheng, Y.-C., Kemeny, N., Bertino, J. R. & Banerjee, D. (2009). *Mol. Cancer Ther.* **8**, 1037–1044.
- Jensen, K. S., Johansson, E. & Jensen, K. F. (2007). *Biochemistry*, **46**, 2745–2757.
- Jong, A., Yeh, Y. & Ma, J. J. (1993). *Arch. Biochem. Biophys.* **304**, 197–204.
- Labesse, G., Benkali, K., Salard-Arnaud, I., Gilles, A. M. & Munier-Lehmann, H. (2011). *Nucleic Acids Res.* **39**, 3458–3472.
- Lee, M.-J., Chien-Liang, L., Tsai, J.-Y., Sue, W.-T., Hsia, W.-S. & Huang, H. (2010). *Arch. Microbiol.* **192**, 739–746.
- Liou, J.-Y., Dutschman, G. E., Lam, W., Jiang, Z. & Cheng, Y.-C. (2002). *Cancer Res.* **62**, 1624–1631.
- Marco-Marín, C., Escamilla-Honrubia, J. M. & Rubio, V. (2005). *Biochim. Biophys. Acta*, **1747**, 271–275.
- Marco-Marín, C., Gil-Ortiz, F. & Rubio, V. (2005). *J. Mol. Biol.* **352**, 438–454.
- Matthews, B. W. (1968). *J. Mol. Biol.* **33**, 491–497.
- Meier, C., Carter, L. G., Sainsbury, S., Mancini, E. J., Owens, R. J., Stuart, D. I. & Esnouf, R. M. (2008). *J. Mol. Biol.* **381**, 1098–1105.
- Meyer, P., Evrin, C., Briozzo, P., Joly, N., Bârz, O. & Gilles, A. M. (2008). *J. Biol. Chem.* **283**, 36011–36018.
- Müller-Dieckmann, H. J. & Schulz, G. E. (1994). *J. Mol. Biol.* **236**, 361–367.
- Murshudov, G. N., Skubák, P., Lebedev, A. A., Pannu, N. S., Steiner, R. A., Nicholls, R. A., Winn, M. D., Long, F. & Vagin, A. A. (2011). *Acta Cryst.* **D67**, 355–367.
- Neuhard, J. & Kelln, R. A. (1996). *Escherichia coli and Salmonella: Cellular and Molecular Biology*, 2nd ed., edited by F. C. Neidhardt, pp. 580–599. Washington: ASM Press.
- Otwinowski, Z. & Minor, W. (1997). *Methods Enzymol.* **276**, 307–326.
- Rossmann, M. G., Moras, D. & Olsen, K. W. (1974). *Nature (London)*, **250**, 194–199.
- Saraste, M., Sibbald, P. R. & Wittinghofer, A. (1990). *Trends Biochem. Sci.* **15**, 430–434.
- Schulz, G. E. (1987). *Cold Spring Harb. Symp. Quant. Biol.* **52**, 429–439.
- Segura-Peña, D., Sekulic, N., Ort, S., Konrad, M. & Lavie, A. (2004). *J. Biol. Chem.* **279**, 33882–33889.
- Serina, L., Blondin, C., Krin, E., Sismeiro, O., Danchin, A., Sakamoto, H., Gilles, A. M. & Bârz, O. (1995). *Biochemistry*, **34**, 5066–5074.
- Serina, L., Bucurenci, N., Gilles, A. M., Surewicz, W. K., Fabian, H., Mantsch, H. H., Takahashi, M., Petrescu, I., Batelier, G. & Bârz, O. (1996). *Biochemistry*, **35**, 7003–7011.
- Shambaugh, G. E. (1979). *Am. J. Clin. Nutr.* **32**, 1290–1297.

- Stevens, A. (1963). *Annu. Rev. Biochem.* **32**, 15–42.
- Terwilliger, T. C., Grosse-Kunstleve, R. W., Afonine, P. V., Moriarty, N. W., Zwart, P. H., Hung, L.-W., Read, R. J. & Adams, P. D. (2008). *Acta Cryst.* **D64**, 61–69.
- Thompson, J. D., Higgins, D. G. & Gibson, T. J. (1994). *Nucleic Acids Res.* **22**, 4673–4680.
- Tong, L. & Rossmann, M. G. (1997). *Methods Enzymol.* **276**, 594–611.
- Tu, J.-L., Chin, K.-H., Wang, A. H.-J. & Chou, S.-H. (2009). *J. Mol. Biol.* **385**, 1113–1126.
- Vagin, A. & Teplyakov, A. (2010). *Acta Cryst.* **D66**, 22–25.
- Yamanaka, K., Ogura, T., Niki, H. & Hiraga, S. (1992). *J. Bacteriol.* **174**, 7517–7526.
- Yan, H. & Tsai, M. D. (1999). *Adv. Enzymol. Relat. Areas Mol. Biol.* **73**, 103–134.
- Zhou, L. & Thornburg, R. (1998). *Arch. Biochem. Biophys.* **358**, 297–302.